Pergamon

Adv. Space Res. Vol. 16, No. 4, pp. (4)99–(4)103, 1995

0273-1177(95)00216-2
0273-1177/95 $9.50 + 0.00

STUDIES OF THE DRAPING AND FLARING ANGLES OF THE MARS AND EARTH MAGNETOTAILS

T.-L. Zhang,* K. Schwingenschuh,* S.M. Petrinec,**
C.T. Russell,** J. G. Luhmann,** H. Rosenbauer,***
M. I. Verigin† and G. Kotova†

* *Space Research Institute, Graz, Austria*
** *IGPP/UCLA, Los Angeles, U.S.A.*
*** *MPIA, Katlenburg-Lindau, Germany*
† *Space Research Institute, Moscow, Russia*

ABSTRACT

Observations of the Mars tail by the Phobos spacecraft have been used to estimate the draping angle of the magnetic field within the tail and the boundary flaring angle. The boundary of the tail is defined by the sudden disappearance of the proton flux as measured by the TAUS ion spectrometer. Solar wind measurements by the TAUS instrument are used to calculate the approximate solar wind dynamic pressure when the spacecraft is within the tail boundary. The average draping angle $(\mathrm{Arcsin}(\sqrt{B_y^2 + B_z^2}/B_T))$ is found to be $27.2° \pm 1.4°$. The draping angle magnitude depends on the solar wind dynamic pressure, but is quite variable. The flaring angle of the tail boundary at $X = -2.5R_M$ has also been calculated from the balance of pressure between the lobe of the Martian tail and the component pressures of the solar wind. The flaring angle depends strongly on the solar wind dynamic pressure, and this dependence is identical to that obtained at the Earth by Petrinec and Russell /1/. However, the magnitude of the flaring angle at Mars at $X = -2.5R_M$ is one-half the value obtained at Earth for $-22.5R_E \leq X - 10R_E$.

INTRODUCTION

Initial observations with the magnetometers on the Phobos mission showed the principally induced nature of the Martian magnetotail /2/ although there is still some uncertainty as to the strength of any intrinsic component of the tail field /3/,/4/. The induced magnetotail forms as a result of the atmospheric mass loading and subsequent draping of passing magnetosheath flux tubes that sink into the wake. In general, planetary bodies without intrinsic magnetic fields, but with substantial atmospheres, are known to possess such cometlike induced magnetotails. To describe the configuration of the magnetotail, we will use the local draping angle and the flaring angle. The local draping angle is the angle between the tail magnetic field and the flow axis X. The flaring angle is the angle between the solar wind flow direction and the tail surface.

In the case of the magnetized planets, the magnetotail is formed due to the tangential stresses of the interaction of the solar wind on an intrinsic magnetic field. However, the strength of the field in the tail, the tail radius and the increase of this radius with distance are governed by the balance between the solar wind pressure on the flaring tail boundary and the mainly magnetic pressure of the tail lobe as originally formulated by Coroniti and Kennel /5/. Petrinec and Russell /1/ showed that the flaring angle of the Earth's tail depends on the distance downtail, X, upstream solar wind dynamic pressure, ρv_{SW}^2, and the B_Z component of the interplanetary magnetic field.

Measurements from the Phobos 2 spacecraft along the circular orbit at 2.8 Mars radii allow us to study the properties of the Mars tail. Previous work includes that of Luhmann et al. /6/ who have conducted a comparative study of the induced magnetotails of Venus, Mars, and Titan. This work indicated that tails of Venus and Mars were similar in their dependence on the IMF strength but that the Mars tail was comparatively wider than that of Venus. More recently Verigin et al. /7/ revealed the compressibilities of the magnetotail boundary.

In this study, we examine the properties of the Martian magnetotail in contrast with the properties of the Earth's tail as studied by Petrinec and Russell /1/. We investigate the dependence of the local draping angle of the tail magnetic field on the upstream solar wind dynamic pressure. We

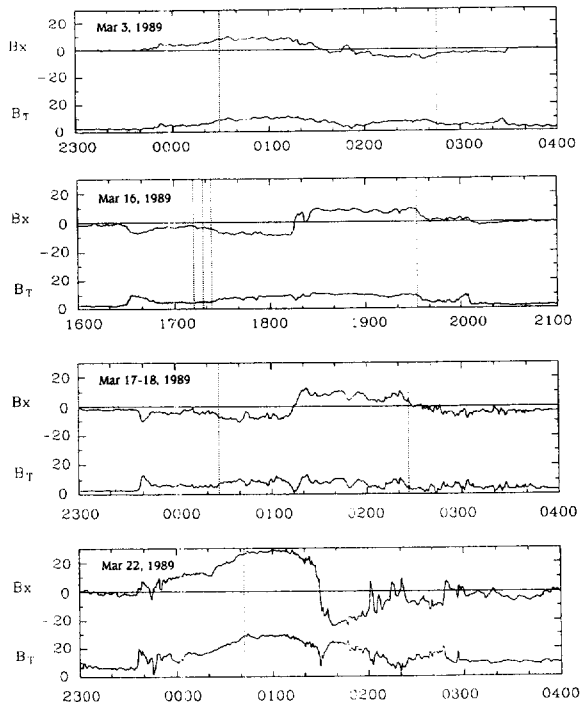

Figure 1 Examples of the magnetotail x component and field magnitude times series observed by the Phobos 2 magnetometer (MAGMA). The data are at 45–sec resolution in Mars Solar Orbital (MSO) coordinates which are analogues to the terrestrial GSE or Solar ecliptic system. The dashed lines are the magnetotail boundaries between draped magnetosheath fields and induced tail lobe fields.

calculate the tail flaring angle from consideration of the balance of the total pressure in the lobes of the magnetotail and the total pressure of the incident solar wind. We show that like at Earth, the flaring angle in Mars' tail depends on ρv_{SW}^2.

OBSERVATIONS

Figure 1 shows examples of the magnetotail x component and field magnitude time series observed by the Phobos 2 magnetometer (MAGMA). The data are at 45–sec resolution in Mars Solar Orbital (MSO) coordinates which are analogous to the terrestrial GSE or Solar ecliptic system. The dashed lines are the magnetotail boundaries between draped magnetosheath fields and induced tail lobe fields. This tail boundary is defined by the sudden disappearance of the proton flux measured by the 2 minute resolution TAUS plasma analyzer.

Of all the circular orbit data, 34 orbits were selected for use. These are all the orbits for which there was sufficient coverage of both the solar wind and the tail to perform the study. The 4 elliptical orbits early in the mission provided little data in the tail and the data were obtained at quite different radial distance. Of orbits used, only one orbit (March 25,1989) is three-axis stabilized data, the rest are despun data. The tail lobe field magnitude is of 12.5±1.1nT, where the error represents a most probable error of the mean. This result is similar to the previous estimate of Luhmann et al. /6/. The average cross-tail field is the average of $\sqrt{B_y^2 + B_z^2}/B_T$. It has a mean value of 5.2±0.3nT.

Figure 2 shows the local draping angle of the magnetic field lines in the tail as a function of the upstream solar wind dynamic pressure. The local draping angle is defined as : arc sin $(\sqrt{B_y^2 + B_z^2}/B_T)$. In this study, we used the orbital averaged cross-tail field and orbital averaged lobe field to calculate the draping angle for each individual orbit. Altogether 34 different draping angles were obtained since only 34 orbits were selected for use. The average of these individual orbital local draping angles is 27.2° ± 1.4°. This value is similar to the value of 23° calculated by Luhmann et. al /6/. The solar wind data are from Phobos 2 TAUS ion spectrometer measurements. We use the recently

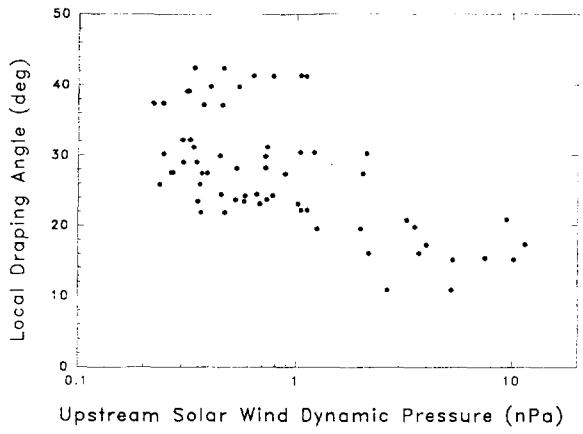

Fig. 2. The local draping angle of the magnetic field lines in the tail as a function of the upstream solar wind dynamic pressure.

recalibrated data /7/. Solar wind measurements are obtained on both inbound and outbound legs just outside the bow shock by averaging over a time interval of 20–30 minutes. For most of the orbits, there are two different solar wind dynamic pressure measurements for each calculated draping angle. Thus 66 data points are shown in Figure 2. It has been shown by Luhmann et al. /6/ that the Venus tail field is more severely draped close to the planet than that at Mars. In Figure 2, we can see that the draping angle at Mars is controlled by the solar wind dynamic pressure but this angle is quite variable. This variability is expected to be due to spatial variations in the draping angle and day-to day variability in the amount of magnetic flux crossing the tail boundary as well as due to variations in the flaring angle of the magnetotail boundary. The tail field seems to be more severely draped for the larger upstream solar wind pressure conditions.

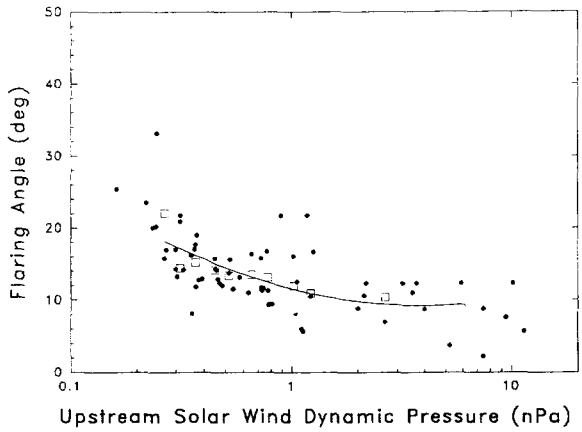

Fig. 3. The tail flaring angle as a function of the upstream solar wind dynamic pressure. The flaring angle is calculated by the the balance of the magnetic pressure in the lobes of the magnetotail and the total pressure of the solar wind. Squares are overlapped averages of 11 data points. The depicted curve is a second order polynomial fit to the average points.

In order to compare with the recent measurements of the shape of the Earth's tail, we plot in Figure 3 the flaring angle as a function of the upstream solar wind dynamic pressure. The flaring angle α is calculated by considering the balance of the total pressure in the lobes of the magnetotail and

the total pressure of the solar wind, as described by:

$$\frac{(B_T^2)_{lobe}}{2\mu_0} = \rho v_{SW}^2 \sin^2\alpha + \frac{(B_T^2)_{SW}}{2\mu_0} + (nk(T_i + T_e))_{SW}$$

We selected the $(B_T)_{lobe}$ by averaging the relatively constant magnetic field data where the tail lobe field was the maximum. Here we have assumed the solar wind electron temperature was twice the ion temperature based on the radial variations observed by the Ulysses spacescraft /8/. For the 34 orbits which were selected in this study, 66 flaring angles were obtained. The flaring angle has a median of 12.6° and mean of 13.6°±0.6°. The scatter is less than that of the draping angle in Figure 2 because the flaring angle, as we have defined it, should not vary across the tail although it will vary along the tail. Our values are obtained all near (but inside) the Phobos orbit at 2.8 Mars radii. We note that this technique avoids some of the problems in other methods of studying the orientation of the boundary. For example a minimum variance analysis of magnetopause normals would suffer from the errors in pointing knowledge of the Phobos spacecraft. A study of the crossing locations would be biassed by the near circular Phobos orbit which would define the average interaction of the tail with a circle quite well but would poorly define the shape of the boundary.
As Figure 3 shows, the flaring angle of the Martian tail varies with the solar wind dynamic pressure. In this plot, squares are averages of each 11 data points, overlapped with the previous average by 5 points. By keeping the number of points in our average constant we maintain statistical accuracy across the plot. The depicted curve is a second order polynomial fit to the average points.

$$\alpha = 11.53 - 7.85 \times log(\rho v_{SW}^2) + 6.63 \times (log(\rho v_{SW}^2))^2$$

for α in degrees and ρv_{SW}^2 in nPa, which has a correlation coefficient of 0.88. To more directly compare with the terrestrial results we compare in Figure 4 our observations at Mars with those obtained by Petrinec and Russell /1/ for the terrestrial tail in the format in which they published their data. Petrinec and Russell /1/ found that this functional dependence produced the most robust tail model. This plot shows averages of 11 points for the Mars data and medians of a much larger sample ($\sim$ 500 points) for the terrestrial data. The correlation coefficient (0.91) is high for the Mars data but there is somewhat less scatter in the larger terrestrial data set because of its smaller statistical error. The variations are almost parallel in this log-log display indicating they have the same power law dependence on the dynamic pressure but the size of the angle is about one-half that at Earth. The Mars values were obtained at about 2.5 R_M behind the planet and terrestrial values at a median distance of 17 R_E /1/. Scaled by the relative sizes of the terrestrial to Martian obstacles to the solar wind these are comparable distances.

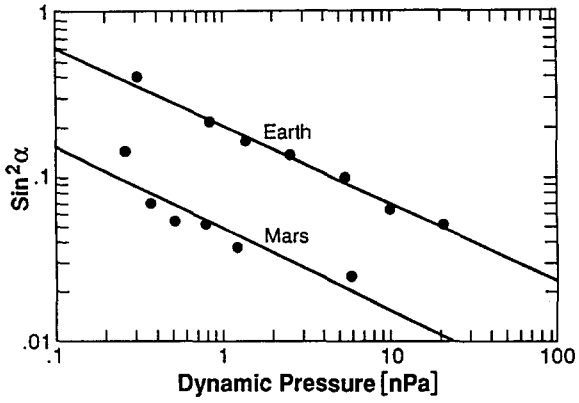

Fig. 4. The square of the sine of the average flaring angle averaged in groups of 11 crossings for Mars plotted versus the solar wind pressure on a log–log plot. The median sine squared flaring angle in groups of about 500 original data points for the Earth are shown for comparison /1/.

CONCLUSIONS

Using the Phobos 2 magnetometer and solar wind data, we have investigated the Martian magnetotail. We find that the local draping angle depends on the upstream solar wind dynamic pressure. The tail field is more severely draped close to the planet for the higher upstream solar wind pressure conditions. We have calculated the flaring angle using the assumption of pressure balance between the lobe field and the solar wind pressures. The tail flaring is strongly controlled by ρv_{SW}^2. Comparing with the Earth tail observations, we find that the Mars magnetotail is similar to the Earth's tail in its dependence on the pressure of the solar wind, but the flaring angle at 2.8 R_M is about one-half the value seen at the Earth at 17 R_E. In order to obtain the same flare at the same dynamic pressure in the Earth's tail one would have to move down tail to 31 R_E according to the relationship found by Petrinec and Russell /1/. This difference should not be taken to be proof of the induced origin of the Martian magnetotail since little has been known from simulations or observations of induced magnetotails as to how an induced magnetotail should vary with solar wind dynamic pressure. We encourage future such studies with cometary and planetary data as well as more studies of the terrestrial magnetotail at greater radial distances.

ACKNOWLEDGMENTS

The work at Moscow was made possible in part by Grant N MQU000 from the International Science Foundation. The work at UCLA was supported by the National Aeronautics and Space Administration under research grants NAGW-2573 and NAGW-2575.

REFERENCES

1. S. M. Petrinec, and C. T. Russell, An empirical model of the size and shape of the near-Earth magnetotail, *Geophys. Res. Lett., 20*, 2695, 1993.
2. Ye. Yeroshenko, W. Riedler, K. Schwingenschuh, J. G. Luhmann, M. Ong, and C. T. Russell, The magnetotail of Mars: Phobos observation, *Geophys. Res. Lett., 17*, 885, 1990.
3. D. W. Möhlmann, J. Rustenbach, K. Schwingenschuh, J. Kurts, U. Motschmann, T. Roatch, K. Sauer and H. I. M. Lichtenegger, The question of an internal Martian magnetic field, *Planet. Space Sci., 39*, 83, 1991.
4. E. Dubinin, R. Lundin, and K. Schwingenschuh, Solar wind electrons as tracers of the Martian magnetosphere topology, *J. Geophys. Res.*, submitted, 1994.
5. F. V. Coroniti, and C. F. Kennel, Changes in magnetospheric configuration during the substorm growth phase, *J. Geophys. Res., 77*, 3361, 1972.
6. J. G. Luhmann, C. T. Russell, K. Schwingenschuh, and Ye. Yeroshenko, A comparison of induced magnetotails of planetary bodies: Venus, Mars, and Titan, *J. Geophys. Res., 96*, 11,199, 1991.
7. M. I. Verigin, K. I. Gringauz, G. A. Kotova, A. P. Remizov, N. M. Shutte, H. Rosenbauer, S. Livi, A. Richter, W. Riedler, K. Schwingenschuh, K. Szego, I. Apathy, and M. Tatrallyay, The dependence of the Martian magnetopause and bow shock on solar wind ram pressure according to Phobos 2 TAUS ion spectometer measurements, *J. Geophys. res., 98*, 1303, 1993.
8. S. J. Bame, J. L. Phillips, D. J. McComas, J. T. Gosling, and B. E. Goldstein, The Ulysses solar wind plasma investigation: Experiment description and initial in-exliptic results, in *Solar Wind Seven,* edited by E. Marsch and R. Schwenn, 139-142, Pergamon, 1992.